Proceedings of the LIV Zakopane School of Physics, Breaking Frontiers, Zakopane, Poland, May 21–25, 2019

Application of Synchrotron Radiation Based X-ray Reflectometry in Analysis of TiO_2 Nanolayers, Unmodified and Irradiated with Xe^{q+} Ions

R. Stachura[a,*], A. Kubala-Kukuś[a,b], D. Banaś[a,b], I. Stabrawa[a,b], K. Szary[a,b], P. Jagodziński[a], G. Aquilanti[c], I. Božičević Mihalić[d], M. Pajek[a], J. Semaniak[a] and M. Teodorczyk[e]

[a]Institute of Physics, Jan Kochanowski University, Świętokrzyska 15, 25-406 Kielce, Poland
[b]Holycross Cancer Center, S. Artwińskiego 3, 25-734 Kielce, Poland
[c]Elettra — Sincrotrone Trieste, s.s. 14, km 163.5 in Area Science Park, 34149 Basovizza, Trieste, Italy
[d]Rudjer Boskovic Institute, Bijenicka cesta 54, 10000 Zagreb, Croatia
[e]Institute of Electronic Materials Technology, Wólczyńska 133, 01-919 Warszawa, Poland

In this work synchrotron radiation based X-ray reflectometry method was applied for determination of morphology of TiO_2 nanolayers, unmodified, and irradiated with low energy highly charged Xe^{q+} ions. Using the synchrotron radiation based X-ray reflectometry technique density, thickness, and roughness of the TiO_2 nanolayers were determined. The results showed that the thicknesses of the nanolayers obtained with synchrotron radiation based X-ray reflectometry method agree within the experimental uncertainty with the declared thicknesses. Moreover, the density of the nanolayers is much lower than density of the bulk TiO_2 due to their nanometer thickness. The results obtained for irradiated samples suggest possible amorphization and smoothening of the TiO_2 nanolayers surface due to interactions of the highly charged ions.

DOI: 10.12693/APhysPolA.137.38

PACS/topics: titanium dioxide, nanolayers, highly charged Xe ions

1. Introduction

The modification of the nanolayers and production of surface nanostructures on metals, semiconductors, and oxides are of great importance in many fields of science, for example, to develop new production technologies of electronics systems with nanometer dimensions [1–4]. Among many tested materials, the studies of the surface modification of titanium and titanium oxides are particularly important because of their widespread use in biomedical devices and components [5]. One of the well-known possibilities of surface modification is irradiation and implantation of a surface with low energy (eV–keV) single charged ions. Such ions dissipate their kinetic energy on, or near to, the surface, which results in defect creation and erosion (sputtering, smoothing, roughening) of material at the surface and can lead to change of electrical, optical, and chemical properties of the irradiated surface [6, 7].

One of the promising future alternatives for creation of surface nanostructures is the modification of surfaces by an impact of single (i.e. each ion creates nanostructure) low-energy (slow) highly charged ions (HCI). Highly charged ions are characterized by additional (to their kinetic energy) potential energy, which for example for Xe^{50+} is equal to $\approx$ 100 keV, i.e. $\approx$ 8400 times higher than that of Xe^{1+}. Consequently, for very slow (eV–keV) HCI, the potential energy can be much higher than kinetic energy and the interaction of such ions with a surface can be dominated by the potential energy. This energy is deposited on a small surface area, along the first few nanometers below the target surface, leading to creation of various surface nanostructures, such as hillocks, pits, and craters [8, 9]. The size and volume of the nanostructures depend strongly on the kinetic and potential energy deposited by the ions. The studies currently performed in this topic concentrate mainly on fundamental understanding of the mechanisms of the surface modifications [8, 9]. For this purpose more systematic measurements at different materials, both as a bulk and nanolayer, and for various type of highly charged ions are needed.

In this study, we use synchrotron radiation (SR) induced X-ray reflectometry (XRR) method for determination of surface properties of titanium oxide nanolayers deposited on Si substrate, unmodified and irradiated with low-energy highly charged xenon ions. Generally, the XRR method is surface sensitive analytical technique for investigation of the near surface regions of variety of materials including single crystals, polycrystalline materials, polymers, organic materials, and fluids [10]. The XRR uses the effect of total external reflection of X-rays from bulk and layered samples. Specular reflection of

*corresponding author; e-mail: regina.stachura06@gmail.com

X-rays on such samples, above critical angle of total reflection, gives rise to the intensity oscillations of the reflected beam, so-called Kiessig fringes [11]. These oscillations are results of specular reflection of X-rays from different interfaces (e.g., substrate–layer and layer–air or layer–layer) of a sample and further interference of the reflected X-rays. A full reflectometry pattern obtained for the reflection angles from 0 to about 5 degrees allows the measurement of the layers thickness, density profiles of near surface regions and roughness of the substrate and layers surfaces. The main advantage of SR-XRR over the standard X-ray tube induced XRR is better beam geometry and much higher intensity of the X-ray beam and thus much better quality of the reflectivity curves.

The results presented in this paper are part of a broader research aimed at investigation of the possibility of analysis of thin films modified with low-energy highly charged ions using grazing-angle X-ray techniques: reflectometry, diffraction, and X-ray fluorescence.

2. Experiment

2.1. Samples description

In this work TiO_2 nanolayers with declared thickness 25, 50, and 75 (± 2) nanometers, deposited on Si substrates with standard $\langle 111 \rangle$ orientation, are studied. The nanolayers were prepared at Institute of Electronic Materials Technology (ITME Warsaw, Poland) by e-beam deposition in the INTEGRITY 29 system (Denton Vacuum) under high vacuum conditions (4–5×10^{-7} mbar). 4N purity materials were used as the targets. The thickness of layer was checked using surface profilometer Dektak 150 (Veeco Instruments Inc.). Before the irradiation the samples were investigated with grazing incident X-ray diffraction which showed that the nanolayers have uniform polycrystalline structure [12].

2.2. Xe irradiation

The nanolayers were implanted with low-energy highly charged Xe^{q+} ($q = 25, 35$) ions, at the Kielce EBIS facility (Jan Kochanowski University, Kielce, Poland) [13]. The xenon ions were obtained from an electron beam ion source EBIS-A. The source supplies a wide range of slow highly charged ions from bare ions of light elements to Ne-like and Ar-like ions of high-Z elements. In the presented experiment, isotopically pure highly charged Xe^{q+} ions were extracted from the EBIT and after selecting ion in the dipole magnet the ions were focused with Einzel lens system onto a sample. The samples were first placed in a loading chamber pumped to about 10^{-7} mbar, and then transmitted to the experimental chamber under UHV. The vacuum in the experimental chamber was around 2–5×10^{-8} mbar. The ion charge and kinetic energy were $q(E) = 25+$ (200 keV) and $35+$ (280 keV). The ion beam fluence was around 4×10^{10} ions/cm^2, therefore on relatively low level, compared to the typical (10^{15} ions/cm^2) fluences used in the ion implantation.

TABLE I

Parameters of the Xe^{q+} ion beams used in the presented studies. The values of the ion range and straggle were simulated using SRIM code [14].

Charge state ($q+$)	Kinetic energy [keV]	Fluence $\times 10^{10}$ [ions/cm^2]	Range [nm]	Straggle [nm]
25+	200	4.0	94	25
35+	280	4.1	119	34

As a result, the main challenge of the performed research is analysis of the modification of a nanolayer surfaces in the regime where the interaction of HCI with a surface leads to creation of separate nanostructures. This condition is fulfilled for the low fluence of the highly charged ion beam. Table I summarizes the information about the Xe^{q+} ion beams used for sample irradiation in the presented studies. The table also presents the values of ion beam range and straggle, simulated using SRIM code [14].

2.3. XRR measurements

The synchrotron radiation based X-ray reflectometry measurements were performed at Elettra Synchrotron in Trieste, at X-ray fluorescence (XRF) beamline [15, 16]. In this experimental setup the X-ray beam, monochromatized using medium energy multilayer in combination with 130 μm of carbon (C) and 15 μm aluminium (Al) filters of a resolving power 5×10^{-3}, has size of 200 μm $\times$ 100 μm (horizontal $\times$ vertical) and an angular divergence of 0.15 mrad. The photon flux is on the level about 2.5×10^{11} photons/s (at 5500 eV, machine mode 2 GeV). The XRR measurements are performed in ultra-high vacuum chamber, operated in partnership with the International Atomic Energy Agency. The beamline end station is equipped with three motorized stages for the alignment of the chamber with respect to the synchrotron beam, a seven-axis motorized manipulator for positioning the sample and the detectors: two silicon drift detectors (SDDs) for XRF and XRR measurements, three Si photodiodes as X-ray monitoring detectors (300 μm thickness, no slit/vertical slit of 100 μm/vertical slit of 200 μm). In the XRR measurements presented in this work, the studied samples were irradiated by X-ray beam of 6.0 keV energy, for which the critical angle is 0.3° for Si and 0.389° for TiO_2. In this regime of the energy and angle, the X-ray attenuation length is 22.3 nm in Si and 12.0 nm in TiO_2 [17].

3. Results and discussion

In order to determine the effect of ion irradiation on the surface characteristics of the tested nanolayers, we have first performed the SR-XRR analysis of unmodified layers. The reflectivity patterns measured for bulk Si (substrate) and 25, 50, and 75 nm titanium dioxide

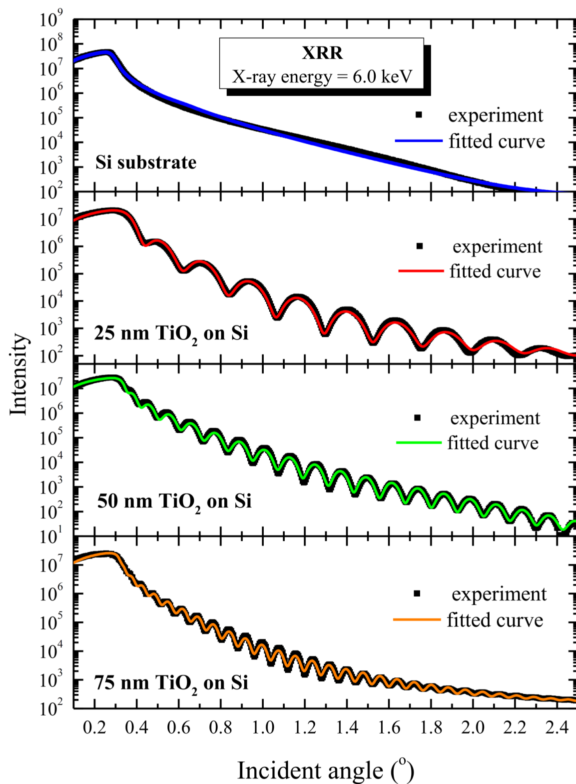

Fig. 1. Reflectivity patterns (black points) measured for the bulk Si (substrate) and 25, 50, and 75 nm titanium dioxide layers deposited on the Si substrate compared with theoretical patterns modelled and fitted using X'Pert Reflectivity 1.3a software (PANalytical).

layers deposited on Si with SR-XRR method are shown in Fig. 1. The measurement for each sample are compared in this figure with results of simulation and fitting performed with X'Pert Reflectivity 1.3a program (PANalytical), which makes use of the Parratt equations for reflectivity [10]. The detailed description of the approach used in the program can be found in [18]. The first step of a reflectivity curve analysis procedure is simulation of the reflectivity curve of a given sample. The key parameters used in the simulations are material parameters, which define the refractive index and linear absorption as a function of depth, and instrumental parameters, which define the incident beam characteristics. The refractive index is a function of the wavelength of the radiation and the electron density of the material. During the simulations, for each angle of incidence, the relative reflected intensity is calculated following a recursive formula which combines the reflected and transmitted amplitudes layer-by-layer throughout the whole sample depth [19]. Final density of the layers forming the sample, their thickness and roughness are obtained by fitting the simulated reflectivity curve to the experimental reflectivity pattern. The fits were performed using genetic algorithm (GA), which is described in detail, for example in Ref. [20].

3.1. Unmodified TiO_2 nanolayers

In the fitting procedure of the bulk Si (substrate) XRR curve the X-ray beam energy was assumed to 6 keV, material (Si) thickness was set to 1 mm (infinitely thick for this energy) and initial Si density to 2.33 g/cm^3. The fitting parameters were: density and roughness of the substrate. The fitted curve is presented in Fig. 1 (the top part). From the fit the following parameters were obtained for the substrate: density 2.17 ± 0.24 g/cm^3 and roughness 0.8 ± 0.1 nm. These substrate parameters and their uncertainties were next used for modelling the TiO_2 nanolayers properties. The TiO_2 samples were modelled by creating structure consisting of substrate (Si), main TiO_2 layer and top layer which we generally call TiO_2 (a) + contamination or simply the top layer. This very thin layer ($\approx$ 1–2 nm) consists of amorphous TiO_2 and some organic species like hydrocarbons, alkoxides, or carboxylates, whose concentrations depend on cleanliness of the sample surface, the exposure time to air and atmosphere quality during storage. The findings, presented in Ref. [5], were confirmed by XPS measurements of our samples, i.e., carbon and nitrogen were detected on the TiO_2 surfaces [22]. We also have made the attempt to model our samples with only one layer on the substrate, but it was not possible to obtain an acceptable fit of the reflectivity curves. Finally, in the fitting procedure of the TiO_2 nanolayers the X-ray beam energy was set to 6 keV, initial nanolayer thicknesses were set to 25, 50, and 75 nm, respectively, and initial TiO_2 density to 4.0 g/cm^3. The initial top layer density was set to 2.0 g/cm^3 and the layer thickness to 2 nm. The initial roughness of TiO_2 layer and the top layer were set to 1 nm. The fitting parameters were the following: densities of TiO_2 and top layers, thickness and roughness of the layers. As a result of the modelling and fitting of the reflectivity curves with different thicknesses, a very good agreement between experimental and theoretical curves have been obtained (see Fig. 1). The results of the fits can be summarized as follows: the densities of the TiO_2 obtained for different nanolayer thicknesses are equal within the uncertainties (3.2 ± 0.3 g/cm^3), but as expected for nanolayers, they have lower density than density of bulk TiO_2 (3.78 g/cm^3 — anatase, 4.23 g/cm^3 — rutile); the density of the top layer was in the range 1.6–2.4 g/cm^3 and thus much lower than the density of the TiO_2 nanolayer. The rest of the fitted parameters are presented in Fig. 2. As it can be seen on the top part of this figure, fitted thicknesses of the titanium dioxide layers agree well with the thickness declared by manufacturer of the samples. We have additionally estimated the nanolayers thickness using, so-called, direct and Fourier methods. In the direct method a layer thickness t is calculated by comparison of angular position of two neighbouring fringes using the following formula [19]:

$$\lambda = 2t\left(\sqrt{\cos^2\theta_c - \cos^2\theta_2} - \sqrt{\cos^2\theta_c - \cos^2\theta_1}\right),$$

where λ is wavelength, θ_c is critical angle, θ_1 is first fringe, θ_2 is second fringe.

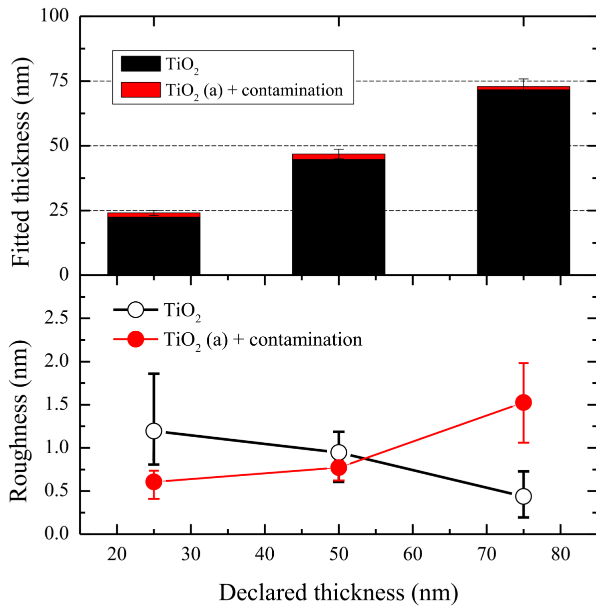

Fig. 2. The thickness and roughness of the nanolayers obtained from the fit of the measured reflectivity curves depicted as a function of declared thicknesses of the TiO_2 nanolayers.

TABLE II

Thickness of the considered nanolayers calculated using different methods. The values are for TiO_2 nanolayers.

Thickness	Full fit	Fourier method	Direct method
25 ± 2 nm	22.4 ± 0.2 nm	23.6 ± 1.2 nm	22.9 ± 14 nm
50 ± 2 nm	44.7 ± 0.4 nm	46.0 ± 2.3 nm	43.8 ± 3.5 nm
75 ± 2 nm	71.6 ± 1.9 nm	70.1 ± 3.5 nm	68.3 ± 5.1 nm

The Fourier analysis performs a fast Fourier transform (FFT). The original $(\theta,\ I)$ data are transferred into $(Q,\ I)$ data [21]:

$$Q(\theta) = \frac{4\pi}{\lambda\left[\cos^2(\theta_c) - \cos^2(\theta)\right]^{1/2}},$$

where Q is scattering momentum, I is intensity, λ is wavelength.

The thickness of a layer can be estimated with this method by finding a peak in the dependence of the Fourier magnitude on the sample thickness [21]. It should be stated here that the direct Fourier methods, due to their methodology (the fringe position estimation), are sensitive to top layer thickness. As a result the contribution of the top layer is within the experimental error of the results.

Generally, the thicknesses obtained from the reflectivity curve using different methods agree well with the declared thicknesses (the biggest differences are for 50 nm nanolayer), but the estimated uncertainties of the analysis are the smallest for simultaneous (full) fit of the whole reflectivity pattern (see Table II).

In the bottom part of Fig. 2 the fitted roughness for TiO_2 and the contamination layers are presented as a function of the nanolayer thickness. The results suggest that the roughness of the TiO_2 layers decrease with the nanolayer thickness, while the roughness of the contamination layer increase with the nanolayer thickness.

3.2. HCI irradiated TiO_2 nanolayers

Irradiated TiO_2 nanolayers were modeled in the same way as unmodified ones, i.e., using two layers, main TiO_2 layer and thin top layer consist of amorphous TiO_2 and the contaminations. In the fitting procedure of the TiO_2 nanolayers modified with HCI xenon, the X-ray beam energy was set to 6 keV, initial nanolayer thickness to 75 nm, and initial TiO_2 density to 3.2 g/cm^3 (obtained for unmodified layers fitting). The initial top layer density was set to 2.0 g/cm^3 and the layer thickness to 2 nm. The initial roughness of TiO_2 layer and top layer were set to 1 nm. The fitting parameters were the following: densities of TiO_2 and the top layers, thickness and roughness of the layers. The results of the fitting procedure are presented in Fig. 3 and in Table III. The lower (Lo) and upper (Up) values of the parameters presented in Table III were obtained using error analysis performed according to a procedure described in [23]. In general, in this procedure for each parameter, the fit value, being the summed differences between the intensities of each measured and simulated point (also called a "chi" value), is calculated for incremental changes of this parameter while the other parameters are kept unchanged. The parameter value range is centered at the start (fitted) value.

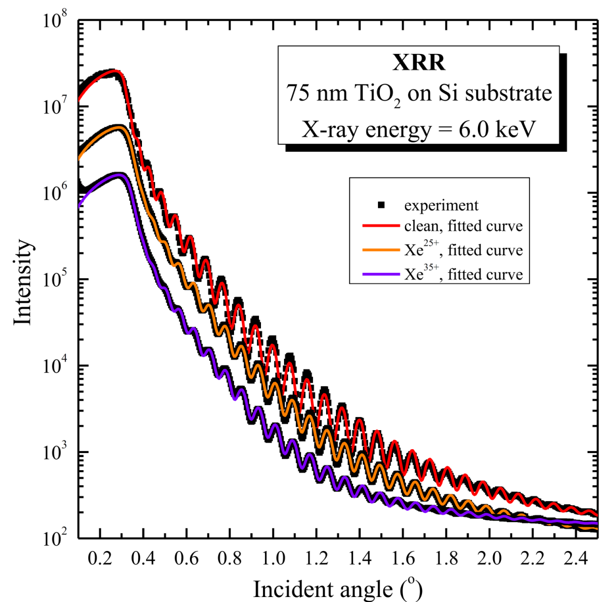

Fig. 3. Reflectivity patterns (black points) measured for 75 nm titanium dioxide layer deposited on the Si substrate irradiated with highly charged xenon ions compared with theoretical patterns modelled and fitted using X'Pert Reflectivity 1.3a software (PANalytical).

TABLE III

Density, thickness and roughness of the TiO_2 and the top (TiO_2 amorphous + contamination) layers irradiated with highly charged xenon ions obtained by fitting the experimental reflectivity curves with a modelled theoretical curves.

TiO_2/Si		Density [g/cm^3]	Lo	Up	Thickness [nm]	Lo	Up	Roughness [nm]	Lo	Up
75 nm	TiO_2 (a)	1.66	1.63	1.98	1.29	0.85	1.85	1.53	1.07	1.99
	TiO_2	3.06	2.92	3.36	71.6	69.5	73.5	0.44	0.39	0.68
75 nm Xe^{25+}	TiO_2 (a)	1.69	1.64	2.02	1.39	1.17	1.58	1.23	0.83	1.41
	TiO_2	3.24	3.11	3.25	71.2	69.7	72.7	0.32	0.28	0.40
75 nm Xe^{35+}	TiO_2 (a)	1.27	1.26	1.53	1.77	0.99	1.89	0.95	0.82	1.32
	TiO_2	3.32	3.19	3.40	71.1	68.6	74.2	0.33	0.12	0.36

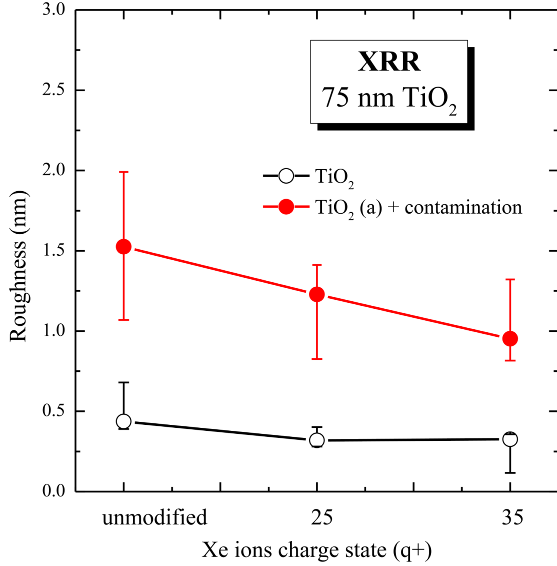

Fig. 4. Comparison of the roughness of the TiO_2 nanolayer unmodified and irradiated with HCI xenon with charge state 25+ and 35+. The presented results are for two layers according to the assumed sample model (see text).

Finally a set of fit values depending on studied parameter value is generated. The Lo and Up values of the parameter are calculated using the range in the fit values below and above the best-fit value, for which the fit value has increased by a chosen percentage (in our case 10%). The error analysis is performed for all fitted parameters [19].

The results of the fits can be summarized as follows: the densities and thicknesses of the TiO_2 layer for unmodified and modified nanolayers are equal within the uncertainties; the density and thickness of the top layer differs slightly only for the sample irradiated with 35+ xenon HCI, the density is lower, while the thickness is greater. This effect suggests amorphization of the top layer, but needs further investigation and comparison of the results with measurements obtained with other grazing-angle X-ray techniques. The roughnesses obtained for unmodified and modified with the HCI nanolayers are shown in Fig. 4. The results are presented for two layers according to the assumed sample model. The results suggest that irradiation of the nanolayers with HCI xenon change the roughness of the outermost nanolayers surface and the change depends on the ion charge state. Such surface smoothing effect is expected for materials irradiated with low energy ions and is the result of beam driven surface relaxation processes [24].

4. Conclusions

In this work SR-XRR method was applied for determination of morphology of TiO_2 nanolayers, unmodified and irradiated with low energy highly charged Xe^{q+} ions. Using the SR-XRR technique density, thickness and roughness of the TiO_2 nanolayers were determined. The TiO_2 nanolayers were modelled by creating structure consisting of substrate (Si), main TiO_2 layer and very thin top layer ($\approx$ 1–2 nm) consisted of amorphous TiO_2 and some organic species like hydrocarbons, alkoxides, or carboxylates, whose concentrations depend on cleanliness of the sample surface, the exposure time to air and atmosphere quality during storage. The method of the sample fitting and the analysis of reflectivity curves was discussed in detail. The results showed that the thicknesses of the TiO_2 nanolayers obtained from the reflectivity curves using direct, Fourier, and full curve fitting methods agree within the experimental uncertainty with the declared thicknesses. As expected, it was found that the measured density of the TiO_2 nanolayers (3.2 ± 0.3 g/cm^3) is much lower than density of the bulk TiO_2 (3.78 g/cm^3 — anatase, 4.23 g/cm^3 — rutile). The results obtained for irradiated samples suggest possible amorphization and smoothening of the TiO_2 nanolayers surface due to HCI–nanolayer surface interaction but this finding needs further investigation and comparison of the results with a measurements obtained with other grazing-angle X-ray techniques. Such analysis is currently in progress.

Acknowledgments

The equipment was purchased thanks to the financial support of the European Regional Development Fund in the framework of the Polish Innovative Economy Operational Program (contract no. WNP-POIG.02.02.00-26-023/08).

This work has been supported by National Science Centre, Poland, under Grant no. DEC-2017/01/X/ST2/01913. The experiment at Elettra has been performed through the project no. 20170407.

References

[1] X. Xiang, X. Zu, S. Zhu, C.F. Zhang, Z.G. Wang, L.M. Wang, R.C. Ewing, *Nucl. Instrum. Meth. Phys. Res. B* **250**, 382 (2006).

[2] L. Zhang, C. Zhang, J. Gou, L.H. Han, Y.T. Yang, Y.M. Sun, Y.F. Jin, *Nucl. Instrum. Meth. Phys. Res. B* **269**, 2835 (2011).

[3] T. Yoshida, S. Niimi, M. Yamamoto, S. Ogawa, T. Nomoto, S. Yagi, *Nucl. Instrum. Methods Phys. Res. B* **365**, 79 (2015).

[4] A. Cusick, M. Lang, F. Zhang, K. Sun, W. Li, P. Kluth, C. Trautmann, R.C. Ewing, *Nucl. Instrum. Methods Phys. Res. B* **407**, 25 (2017).

[5] X. Liu, P. Chu, C. Ding, *Mater. Sci. Eng. R* **47**, 49 (2004).

[6] J.S. Williams, R.G. Elliman, M.C. Ridgway, *Ion Beam Modification of Materials*, Elsevier B.V., North-Holland, 1996.

[7] W.L. Chan, E Chason, *J. Appl. Phys.* **101**, 121301 (2007).

[8] I. Stabrawa, D. Banaś, A. Kubala-Kukuś, K. Szary, J. Braziewicz, J. Czub, Ł. Jabłoński, P. Jagodziński, D. Sobota, M. Pajek, K. Skrzypiec, E. Mendyk, M. Teodorczyk, *Nucl. Instrum. Methods Phys. Res. B* **408**, 235 (2017).

[9] R.A. Wilhelm, A.S. El-Said, F. Krok, R. Heller, E. Gruber, F. Aumayr, S. Facsko, *Prog. Surf. Sci.* **90**, 377 (2015).

[10] L.G. Parratt, *Phys. Rev.* **95**, 359 (1954).

[11] H. Kiessig, *Ann. Phys.* **10**, 769 (1931).

[12] I. Stabrawa, A. Kubala-Kukuś, D. Banaś, G. Pepponi, J. Braziewicz, M. Pajek, M. Teodorczyk, *Thin Solid Films* **671**, 103 (2019).

[13] D. Banaś, Ł. Jabłoński, P. Jagodziński, A. Kubala-Kukuś, D. Sobota, M. Pajek, *Nucl. Instrum. Methods Phys. Res. B* **354**, 125 (2015).

[14] J. Ziegler, M. Ziegler, J. Biersack, *Nucl. Instrum. Methods Phys. Res. B* **268**, 1818 (2010).

[15] W. Jark, D. Eichert, L. Luehl, A. Gambitta, *Proc. SPIE* **9207**, IX 92070G (2014).

[16] A.G. Karydas, M. Czyżycki, J.J. Leani, A. Migliori, J. Osan, M. Bogovac, P. Wróbel, N. Vakula, R. Padilla-Alvarez, R.H. Menk, M. Gol, M. Antonelli, M.K. Tiwari, C. Caliri, K. Vogel-Mikus, I. Darby, R.B. Kaiser, *J. Synchrotr. Radiat.* **25**, 189 (2018).

[17] B.L. Henke, E.M. Gullikson, J.C. Davis, *At. Data Nucl. Data Tables* **54**, 181 (1993).

[18] P.F. Fewster, *X-Ray Scattering from Semiconductors*, 2nd ed., Imperial College Press, 2003, p. 82.

[19] X'Pert Reflectivity manual, PANalytical B.V., 2007.

[20] A.D. Dane, A. Veldhuis, D.K.G. de Boer, A.J.G. Leenaers, L.M.C. Buydens, *Physica B* **253**, 254 (1998).

[21] F. Bridou, B. Pardo, *J. Phys. III (France)* **4**, 1523 (1994).

[22] A. Kubala-Kukuś, D. Banaś, I. Stabrawa, K. Szary, D. Sobota, U. Majewska, J. Wudarczyk-Moćko, J. Braziewicz, M. Pajek, *Spectrochim. Acta B* **145**, 43 (2018).

[23] W.H. Press, S.A. Teukolsky, W.T. Vetterling, B.P. Flannery, *Numerical Recipes in C++*, Cambridge University Press, 2002, Sect. 15.6, p. 699.

[24] F. Frost, R. Fechner, B. Ziberi, J. Völlner, D. Flamm, A. Schindler, *J. Phys. Condens. Matter* **21**, 224026 (2009).